Supporting Information

Assembly of pinwheel/twist shaped chiral lanthanide clusters with rotor structures by annular/linear growth mechanism and their magnetic properties

Bing-Fan Long,[a,+] Yun-Lan Li,[a,+] Zhong-Hong Zhu,[a,] Hai-Ling Wang,[a] Fu-Pei Liang,[a,b,*] and Hua-Hong Zou[a,*]*

[a]School of Chemistry and Pharmaceutical Sciences, State Key Laboratory for Chemistry and Molecular Engineering of Medicinal Resources/Key Laboratory for Chemistry and Molecular Engineering of Medicinal Resources (Ministry of Education of China), Collaborative Innovation Center for Guangxi Ethnic Medicine, School of Chemistry and Pharmaceutical Sciences, Guangxi Normal University, Guilin 541004, P. R. China

[b]Guangxi Key Laboratory of Electrochemical and Magnetochemical Functional Materials, College of Chemistry and Bioengineering, Guilin University of Technology, Guilin 541004, P. R. China

*E-mail (Corresponding author): 18317725515@163.com (Z.-H. Zhu), liangfupei@glut.edu.cn (F.-P. Liang), gxnuchem@foxmail.com (H.-H. Zou).

Keywords: Chiral lanthanide clusters; solvothermal synthesis; annular growth mechanism; linear growth mechanism; magnetic properties

Table of Contents:

Figure S11	Loop curve graph of clusters ***R*-1** and ***R*-2** at 2 K (a, b).
Figure S12	Plots of χ'' *vs.* ν (10−1000 Hz) at 2 K under 500−4000 Oe dc field with a 2 Oe oscillating ac field for cluster ***R*-2** (a); Variable-frequency AC susceptibilities (H = 1000 Oe) of cluster ***R*-2** at different temperatures (b, c) and Cole-Cole plots from AC susceptibilities (d).
Figure S13	Variable-frequency AC susceptibilities (H = 0 Oe) of clusters ***R*-1** (a, b) and ***R*-2** (c, d) at different temperatures.
Figure S14	Arrhenius plots generated from the temperature-dependent relaxation times extracted from the Cole-Cole fits of the AC susceptibilities for clusters ***R*-1** and ***R*-2** under 0 Oe (a, b). Symbols show the extracted times, and the lines are least-squares fits.
Figure S15	Arrhenius plots generated from the temperature-dependent relaxation times extracted from the Cole-Cole fits of the AC susceptibilities for cluster ***R*-2** under 1000 Oe. Symbols show the extracted times, and the lines are least-squares fits.
Figure S16	Plots of $\chi_{\mathrm{m}}T$ versus T for clusters ***S*-1** and ***S*-2** (a, c); M *vs.* H/T plots of clusters ***S*-1** and ***S*-2** (b, d).
Figure S17	Loop curve graph of clusters ***S*-1** and ***S*-2** (a, b) at 2 K.
Figure S18	Temperature-dependent χ' and χ'' AC susceptibilities under 0 Oe DC fields for ***S*-1** and ***S*-2** (a, c); Cole−Cole plots for ***S*-1** and ***S*-2** (b, d).
Figure S19	Temperature-dependent χ' and χ'' AC susceptibilities under 1000 Oe DC fields for ***S*-2** (a); Cole−Cole plots for ***S*-2** (b).
Figure S20	Arrhenius plots generated from the temperature-dependent relaxation times extracted from the Cole-Cole fits of the AC susceptibilities for clusters ***S*-1** and ***S*-2** under 0 Oe (a, b) and ***S*-2** under 1000 Oe (c). Symbols show the extracted times, and the lines are least-squares fits.

Experimental Section

Materials and Measurements.

All chemicals and solvents were analytical grade and were used without further purification. The infrared spectra were carried out on a Pekin-Elmer Two spectrophotometer with pressed KBr pellets. The elemental analyses were determined on a Perkin-Elmer model 240 °C elemental analyzer. The powder X-ray diffraction (PXRD) spectra were measured on a Rigaku D/Max-3c diffractometer with Cu Kα radiation (λ = 1.5418 Å). Thermogravimetric analyses were performed on a PerkinElmer PyrisDiamond TG-DTA instrument under an N_2 atmosphere using a heating rate of 5 °C min^{-1} from room temperature up to 1000 °C. The circular dichroism (CD) spectra were recorded on a JASCO J-1500 spectropolarimeter at room temperature. Magnetic properties were performed on a Superconducting Quantum Interference Device (SQUID) magnetometer. The diamagnetism of all constituent atoms was corrected with Pascal's constant.

X-ray crystallography.

Single-crystal X-ray diffraction (SCXRD) data were collected on a ROD, Synergy Custom DW system, HyPix diffractometer (Cu-Kα radiation and λ = 1.54184 Å) in Φ and ω scan modes. The structures were solved by direct methods, and refined by a full-matrix least-squares method on the basis of F^2 by using *SHELXL*.[1] Anisotropic thermal parameters were applied to all non-hydrogen atoms. Hydrogen atoms were generated geometrically. Highly disordered free solvent molecules were removed using the SQUEEZE function of PLATON. The crystallographic data for the ligand and clusters ***R*-1**, ***S*-1**, ***R*-2** and ***S*-2** are listed in Table S1, and selected bond lengths and angles are given in Table S2−S5. The CCDC reference numbers for the crystal structures of clusters ***R*-1**, ***S*-1**, ***R*-2** and ***S*-2** are 2183488−2183491, respectively.

[1] Sheldrick, G. M. *Acta Crystallogr., Sect. C: Struct. Chem*. **2015**, *71*, 3−8.

The synthesis method.

Synthesis of *R*-1: ***R***-2-hydroxy-2-phenylacetohydrazide (0.1 mmol, 0.0166 g), 2,3-dihydroxybenzaldehyde (0.1 mmol, 0.0138 g), $DyCl_3 \cdot 6H_2O$ (0.5 mmol, 0.1885 g) and triethylamine (80 μL) were dissolved in a mixed solvent of ethanol (1.0 mL) and water (0.2 mL) in a Pyrex tube. The tube was sealed and heated at 80 °C in an oven for one day, then cooled down slowly, yellow block crystals were obtained with a yield of about 60% (based on ***R***-2-hydroxy-2-

phenylacetohydrazide). Elemental analysis theoretical value ($C_{82}H_{160}Cl_8Dy_8N_8O_{60}$): C, 25.90%; H, 4.24%; N, 2.94%; experimental value: C, 25.85%; H, 4.21%; N, 2.92%. Infrared spectrum data (IR, KBr pellet, cm^{-1}): 3324(s), 2984(m), 1613(s), 1457(s), 1400(m), 1263(s), 1207(m), 1065(s), 872(m), 749(m), 701(w), 611(w).

Synthesis of *S*-1: The synthesis method was similar to that for ***R*-1** by using ***S***-2-hydroxy-2-phenylacetohydrazide instead of ***R***-2-hydroxy-2-phenylacetohydrazide. The yield is 60% (based on ***S***-2-hydroxy-2-phenylacetohydrazide). Elemental analysis theoretical value ($C_{88}H_{184}Cl_8Dy_8N_8O_{66}$): C, 26.46%; H, 4.64%; N, 2.80%; experimental value: C, 26.41%; H, 4.62%; N, 2.76%. Infrared spectrum data (IR, KBr pellet, cm^{-1}): 3315(s), 2978(m), 1604(s), 1554(m) 1457(s), 1393(m), 1267(s), 1212(m), 1060(s), 875(m), 746(m), 702(w), 604(w).

Synthesis of *R*-2: ***R***-2-hydroxy-2-phenylacetohydrazide (0.1 mmol, 0.0166 g), 2,3-dihydroxybenzaldehyde (0.1 mmol, 0.0138 g), $Dy(NO_3)_3 \cdot 6H_2O$ (0.5 mmol, 0.1885 g) and triethylamine (80 μL) were dissolved in a mixed solvent of methanol (1.0 mL) and water (0.2 mL) in a Pyrex tube. The tube was sealed and heated at 80 °C in an oven for one day, then cooled down slowly, yellow rhombic crystals were obtained with a yield of about 65% (based on ***R***-2-hydroxy-2-phenylacetohydrazide). Elemental analysis theoretical value ($C_{107}H_{174}Dy_6N_{14}O_{68}$): C, 34.55%; H, 4.71%; N, 5.27%; experimental value: C, 34.53%; H, 4.67%; N, 5.22%. Infrared spectrum data (IR, KBr pellet, cm^{-1}): 3408(s), 2980(m), 1614(s), 1453(s), 1384(s), 1263(s), 1206(m), 1060(s), 872(m), 739(s), 602(w).

Synthesis of *S*-2: The synthesis method was similar to that for ***R*-2** by using ***S***-2-hydroxy-2-phenylacetohydrazide instead of ***R***-2-hydroxy-2-phenylacetohydrazide. The yield is 65 % (based on ***S***-2-hydroxy-2-phenylacetohydrazide). Elemental analysis theoretical value ($C_{107}H_{168}Dy_6N_{14}O_{67}$): C, 34.75%; H, 4.58%; N, 5.30%; experimental value: C, 34.72%; H, 4.53%; N, 5.28%. Infrared spectrum data (IR, KBr pellet, cm^{-1}): 3415(s), 2982(s), 1607(s), 1453(s), 1387(s), 1259(s), 1205(m), 1060(s), 872(m), 738(s), 605(w).

Table S1. Crystallographic data of the clusters ***R*-1**, ***S*-1**, ***R*-2** and ***S*-2**.

	***R*-1**	***S*-1**	***R*-2**	***S*-2**
Formula	$C_{82}H_{160}Cl_8Dy_8N_8O_{60}$	$C_{88}H_{184}Cl_8Dy_8N_8O_{66}$	$C_{107}H_{174}Dy_6N_{14}O_{68}$	$C_{107}H_{168}Dy_6N_{14}O_{67}$
Formula weight	3801.77	3994.02	3719.59	3697.54
T, K	100.00(10)	100.00(10)	100.00(10)	100.00(10)
Crystal system	monoclinic	monoclinic	tetragonal	tetragonal
Space group	$C2$	$C2$	$P4_32_12$	$P4_12_12$
a, Å	19.582(16)	19.561(10)	14.400(10)	14.414(10)
b, Å	18.453(15)	18.409(10)	14.400(10)	14.414(10)
c, Å	19.787(14)	19.748(10)	71.412(5)	71.463(4)
α, °	90	90	90	90
β, °	92.1497(7)	92.095(10)	90	90
γ, °	90	90	90	90
V, Å^3	7145.45(10)	7107.00(6)	14809.2(2)	14848.7(2)
Z	2	2	4	4
D_c, g cm^{-3}	1.559	1.524	1.389	1.469
μ, mm^{-1}	23.877	23.979	16.479	16.514
F(000)	3200.0	3096.0	6024.0	6432.0
2θ range for data collection/°	4.468 to 133.192	4.478 to 154.102	4.95 to 151.65	4.946 to 151.458
Reflns coll.	44229	50425	52013	49848
Unique reflns	12550	14029	14821	14921
R_{int}	0.0453	0.0432	0.0429	0.0449
R_1^a ($I > 2\sigma(I)$)	0.0676	0.0433	0.0449	0.0411
wR_2^b (all data)	0.1765	0.1171	0.1311	0.1122
GOF	1.098	1.073	1.084	1.061
Flack parameter	0.077(9)	0.019(5)	0.015(5)	0.001(2)

$^aR_1 = \Sigma||F_o|-|F_c||/\Sigma|F_o|$, $^bwR_2 = [\Sigma w(F_o^2-F_c^2)^2/\Sigma w(F_o^2)^2]^{1/2}$

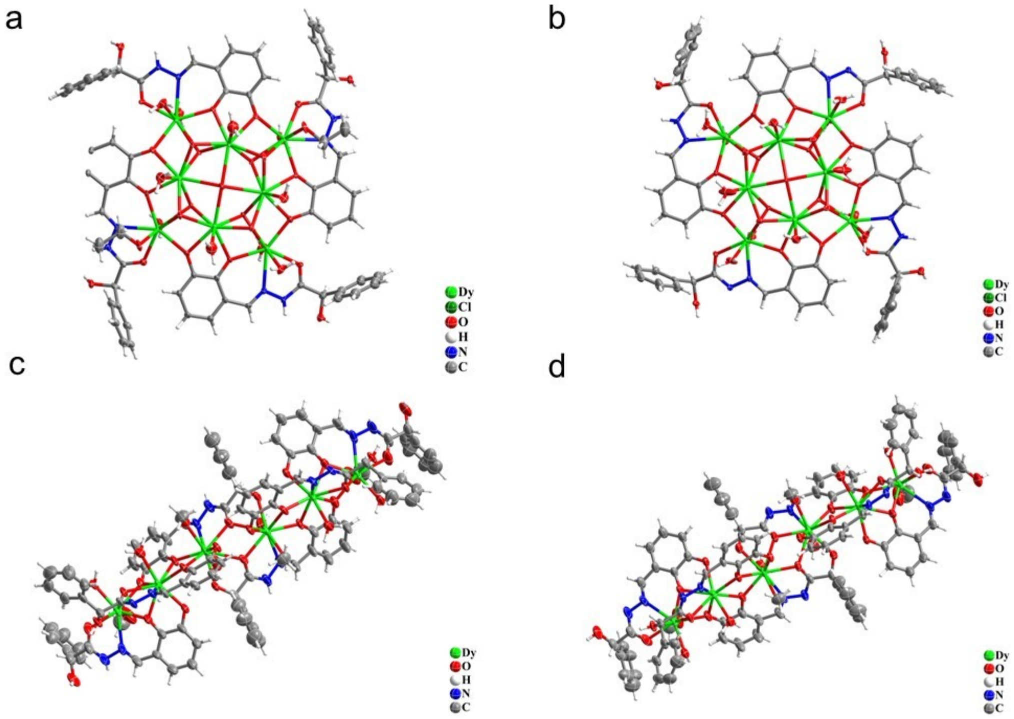

Figure S1. Crystal structures of ***R*-1** (a); ***S*-1** (b); ***R*-2** (c); ***S*-2** (d).

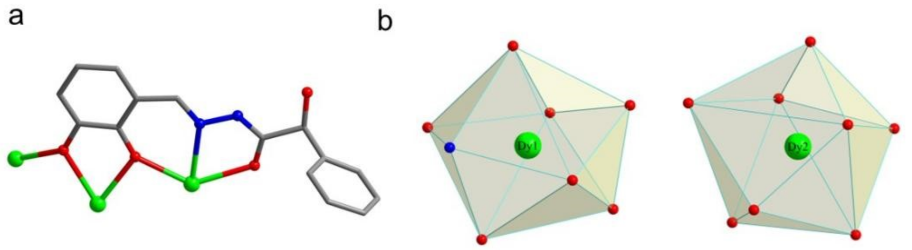

Figure S2. Ligand coordination mode of cluster ***R*-1** (a); Coordination polyhedron around the Dy(III) ions of cluster ***R*-1** (b).

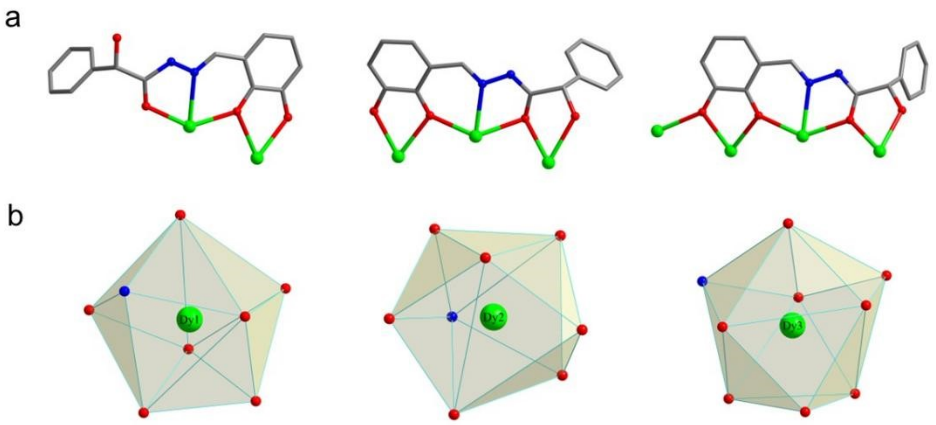

Figure S3. Ligand coordination mode of cluster ***R*-2** (a); Coordination polyhedron around the Dy(III) ions of cluster ***R*-2** (b).

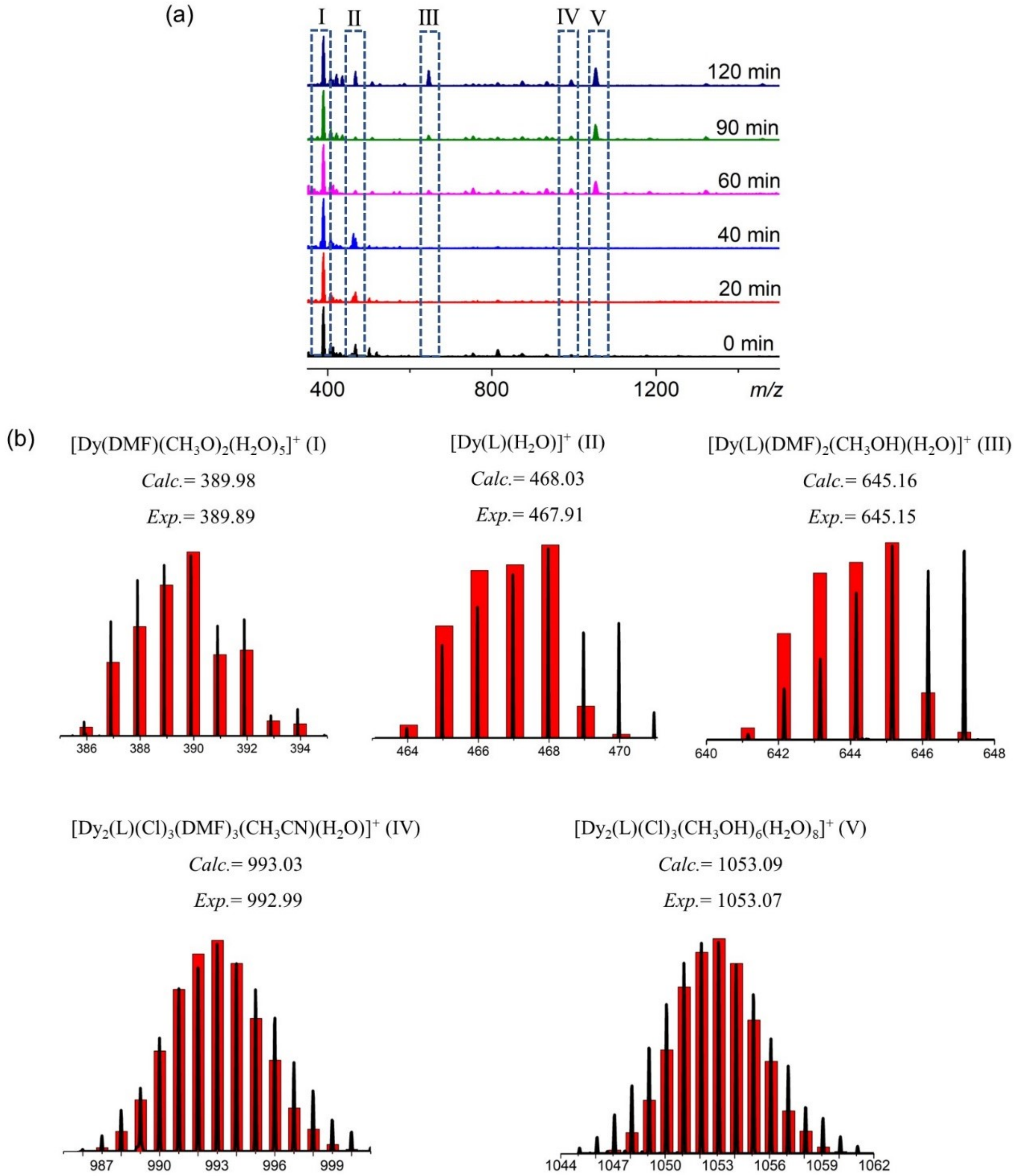

Figure S4. Time-dependent HRESI-MS spectra of the initial cluster ***R*-1** reaction in positive mode (a); Positive HRESI-MS spectra of cluster ***R*-1** in MeOH (0, 20, 40, 60, 90 and 120 min) (b).

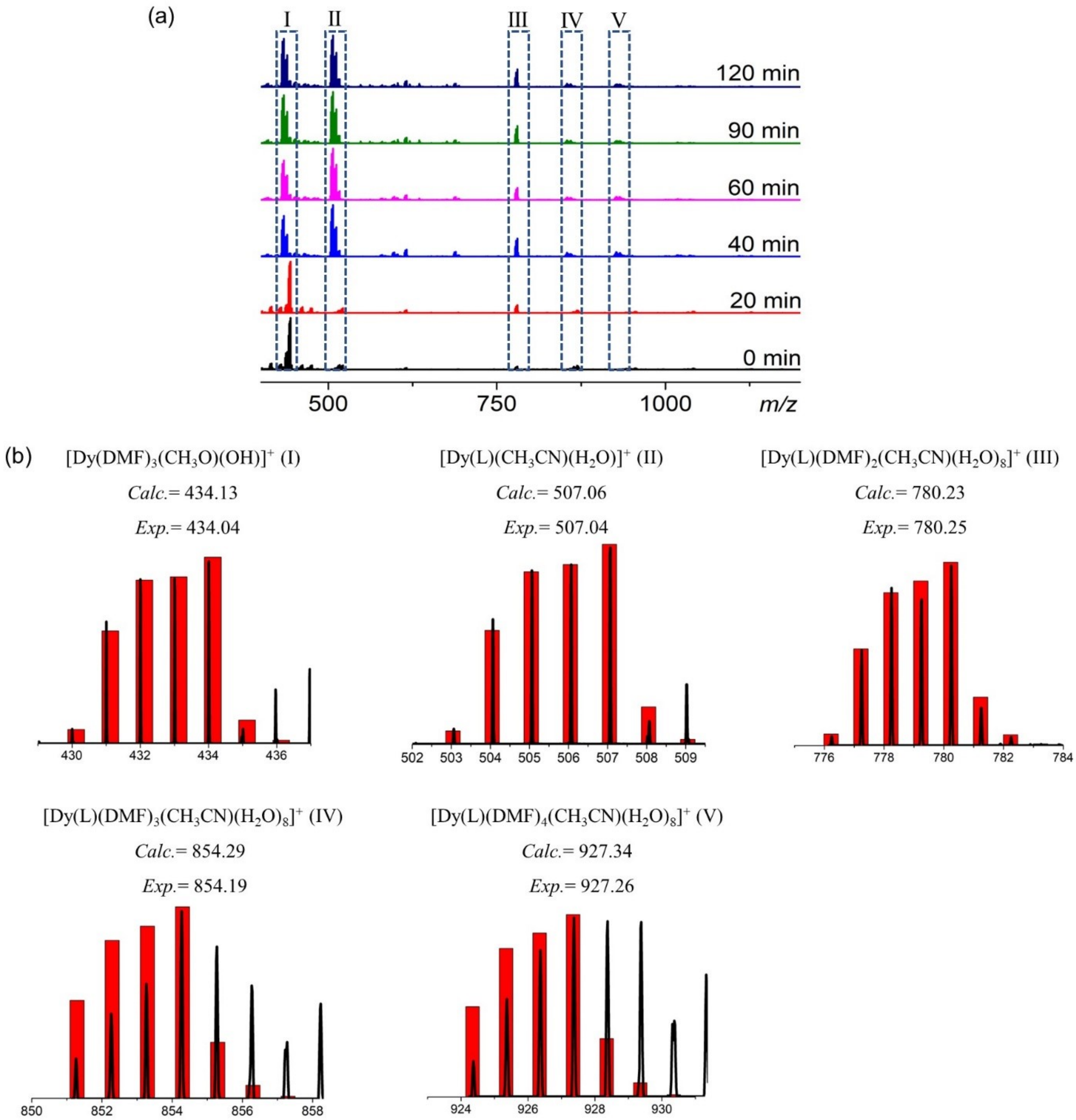

Figure S5. Time-dependent HRESI-MS spectra of the initial cluster ***R*-2** reaction in positive mode (a); Positive HRESI-MS spectra of cluster ***R*-2** in MeOH (0, 20, 40, 60, 90 and 120 min) (b).

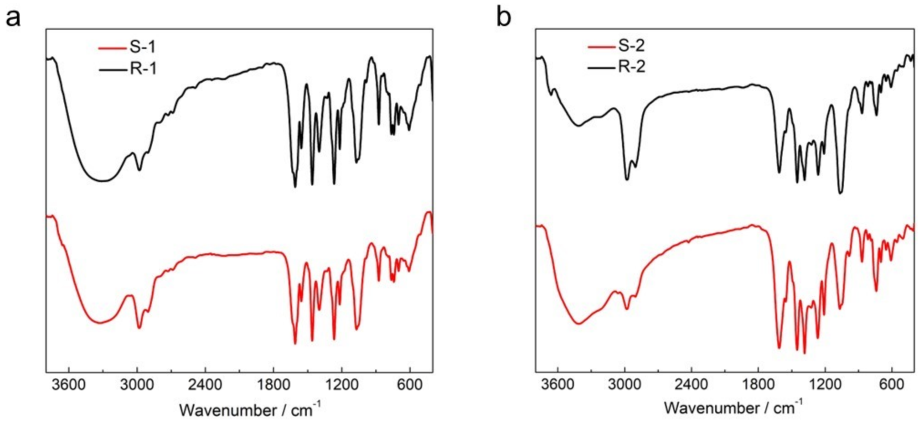

Figure S6. Infrared spectra (IR) of clusters ***R*-1**, ***S*-1**, ***R*-2** and ***S*-2** (a, b).

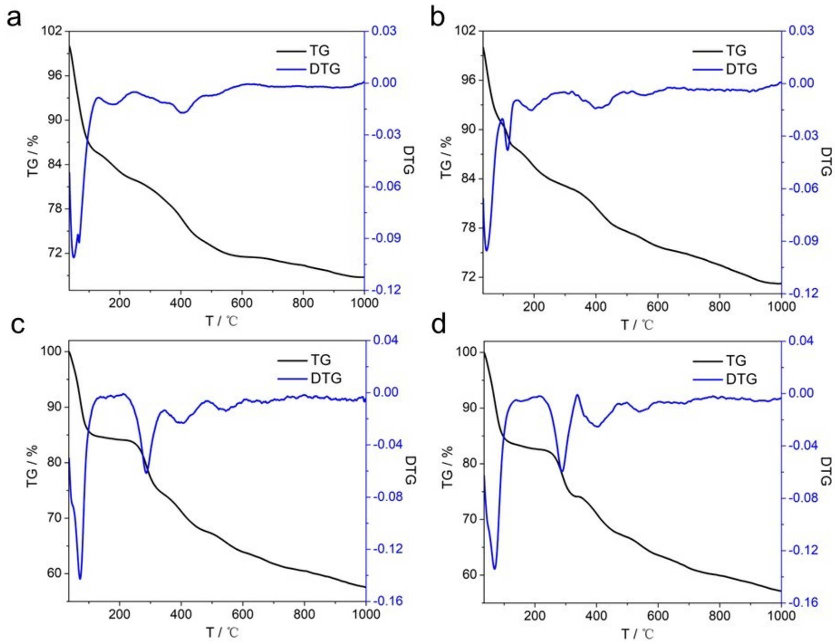

Figure S7. TG curve of clusters ***R*-1**, ***S*-1**, ***R*-2** and ***S*-2** (a–d).

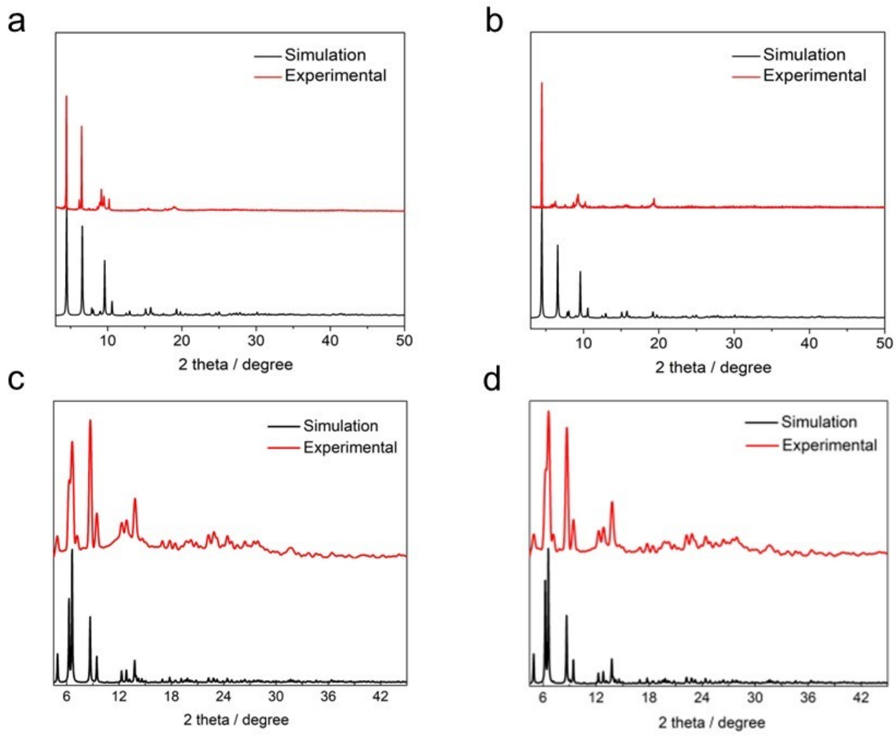

Figure S8. Powder diffraction pattern (PXRD) of clusters ***R*-1**, ***S*-1**, ***R*-2** and ***S*-2** (a–d).

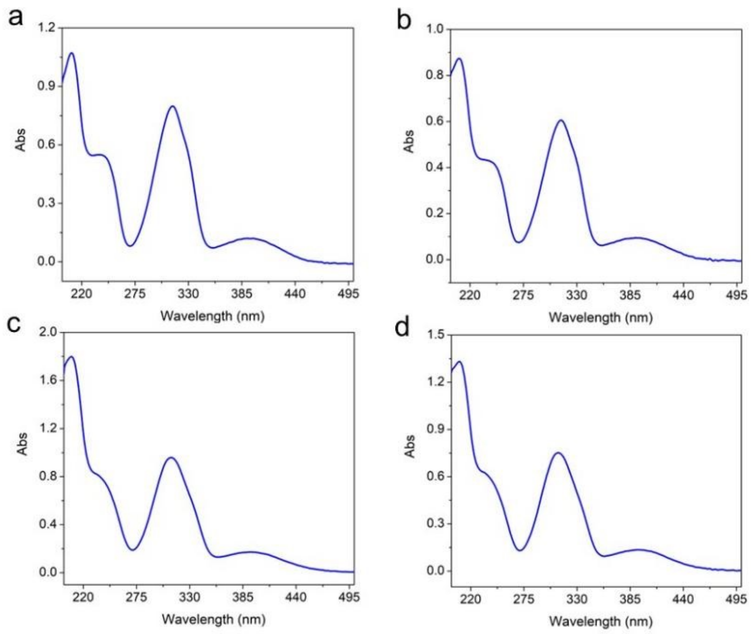

Figure S9. The UV-Vis absorption spectra of clusters ***R*-1**, ***S*-1**, ***R*-2** and ***S*-2** (a–d).

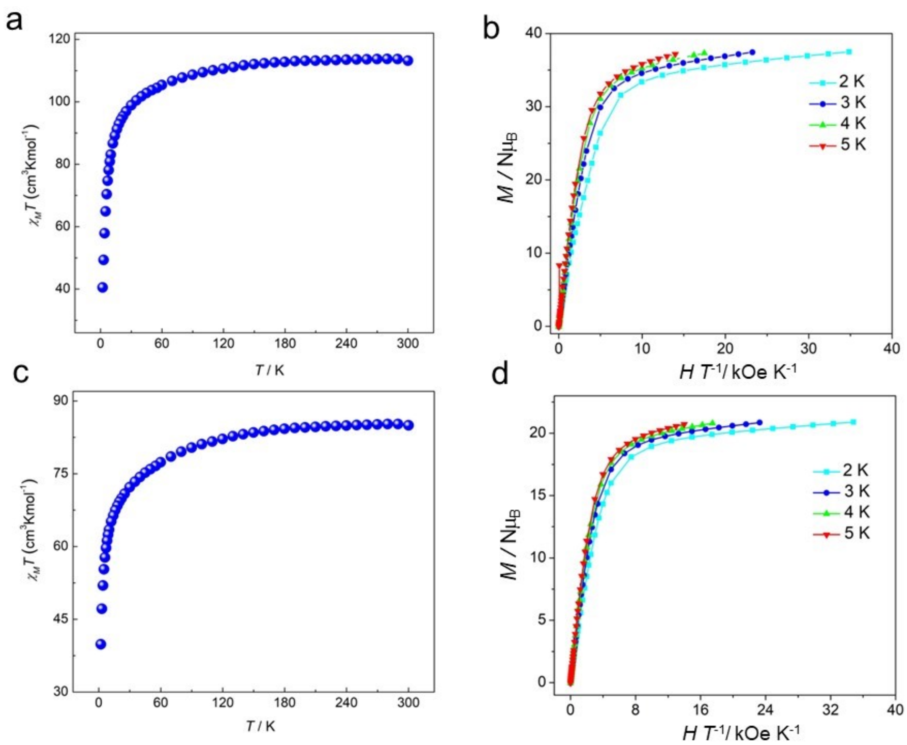

Figure S10. Plots of $\chi_m T$ versus T for clusters ***R*-1** and ***R*-2** (a, c); *M vs. H/T* plots of clusters ***R*-1** and ***R*-2** (b, d).

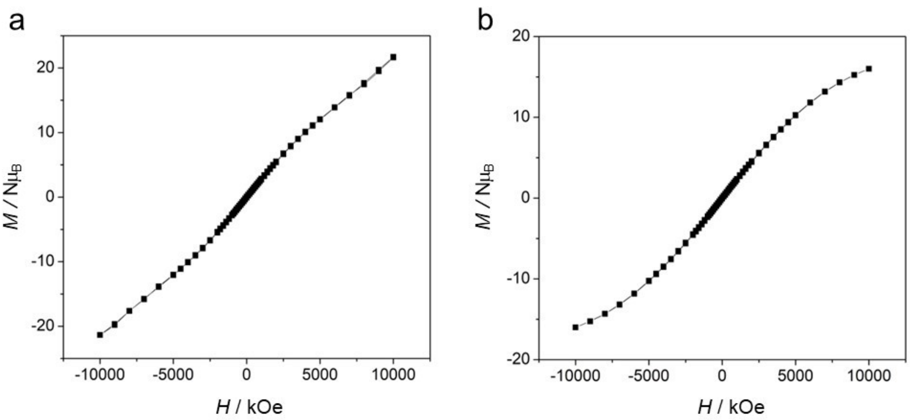

Figure S11. Loop curve graph of clusters ***R*-1** and ***R*-2** (a, b) at 2 K.

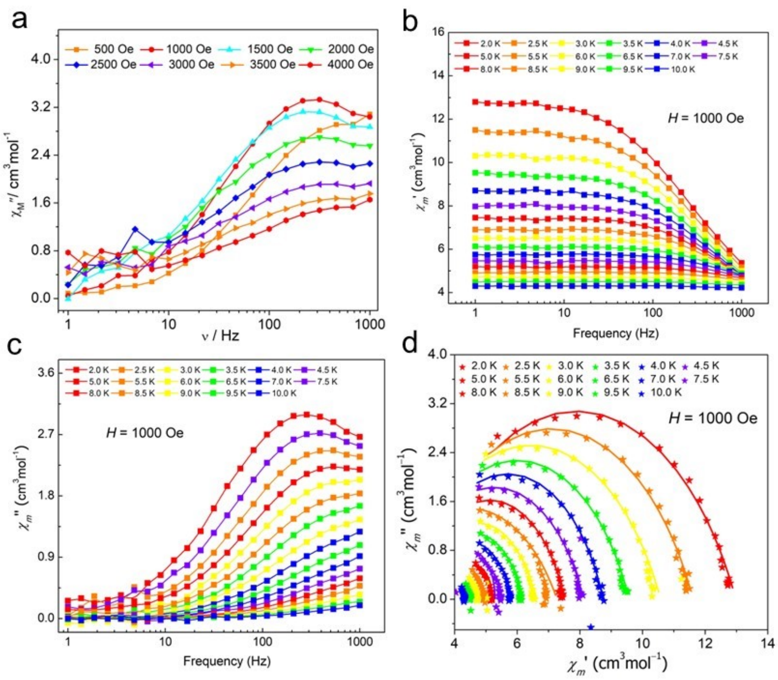

Figure S12. Plots of χ'' *vs.* ν (10−1000 Hz) at 2 K under 500−4000 Oe dc field with a 2 Oe oscillating ac field for cluster ***R*-2** (a); Variable-frequency AC susceptibilities (H = 1000 Oe) of cluster ***R*-2** at different temperatures (b, c) and Cole-Cole plots from AC susceptibilities (d).

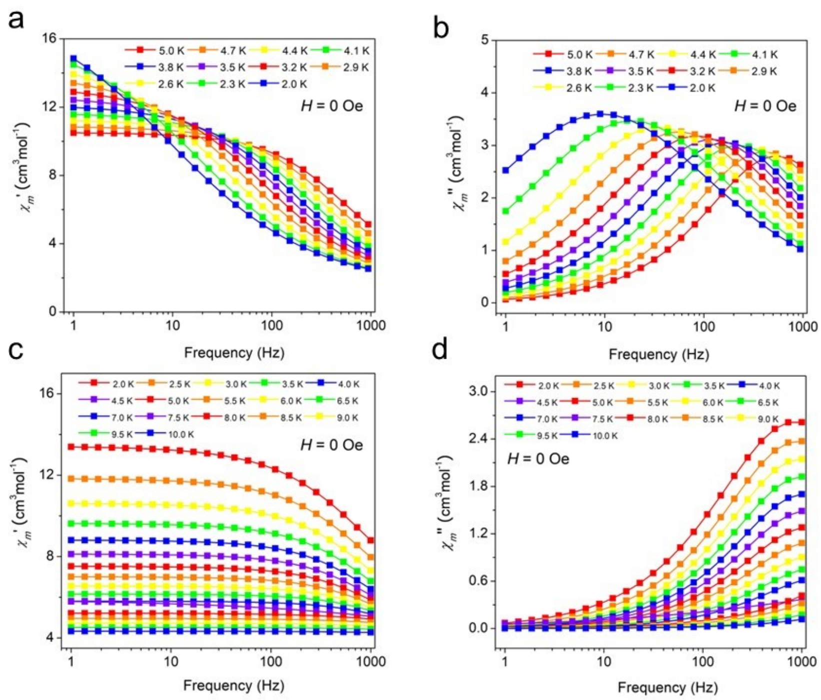

Figure S13. Variable-frequency AC susceptibilities (H = 0 Oe) of clusters ***R*-1** (a, b) and ***R*-2** (c, d) at different temperatures.

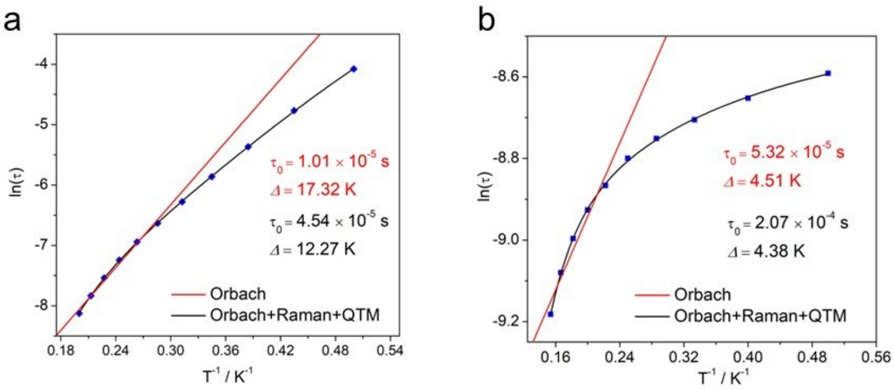

Figure S14. Arrhenius plots generated from the temperature-dependent relaxation times extracted from the Cole-Cole fits of the AC susceptibilities for clusters ***R*-1** and ***R*-2** under 0 Oe (a, b). Symbols show the extracted times, and the lines are least-squares fits.

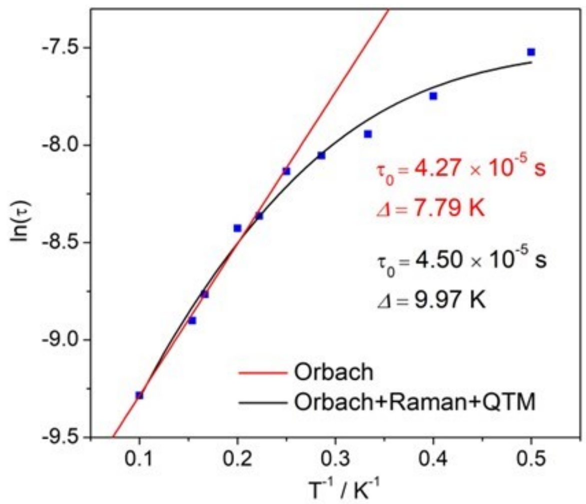

Figure S15. Arrhenius plots generated from the temperature-dependent relaxation times extracted from the Cole-Cole fits of the AC susceptibilities for cluster ***R*-2** under 1000 Oe. Symbols show the extracted times, and the lines are least-squares fits.

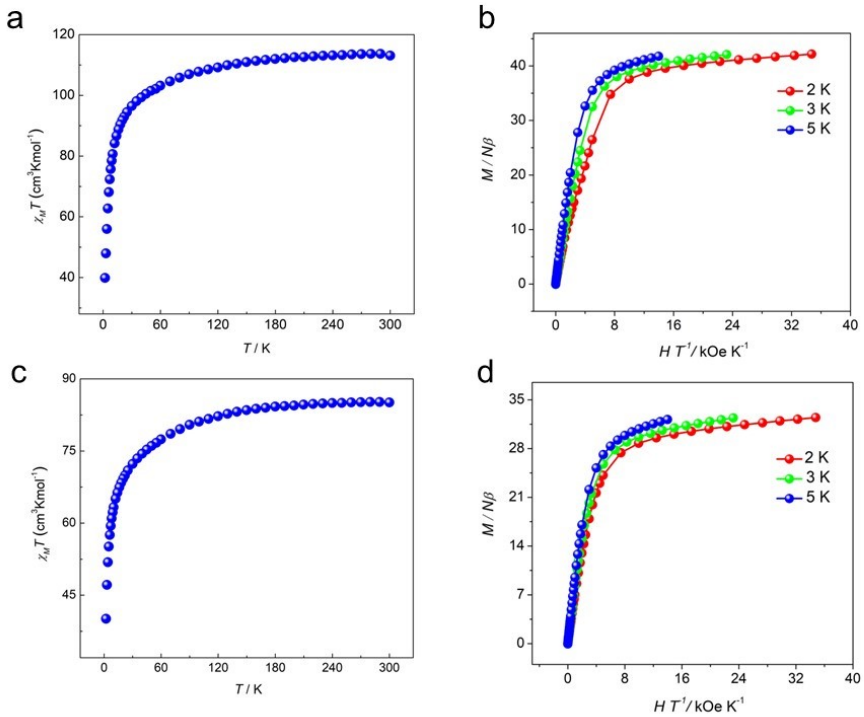

Figure S16. Plots of $\chi_m T$ versus T for clusters ***S*-1** and ***S*-2** (a, c); *M vs. H/T* plots of clusters ***S*-1** and ***S*-2** (b, d).

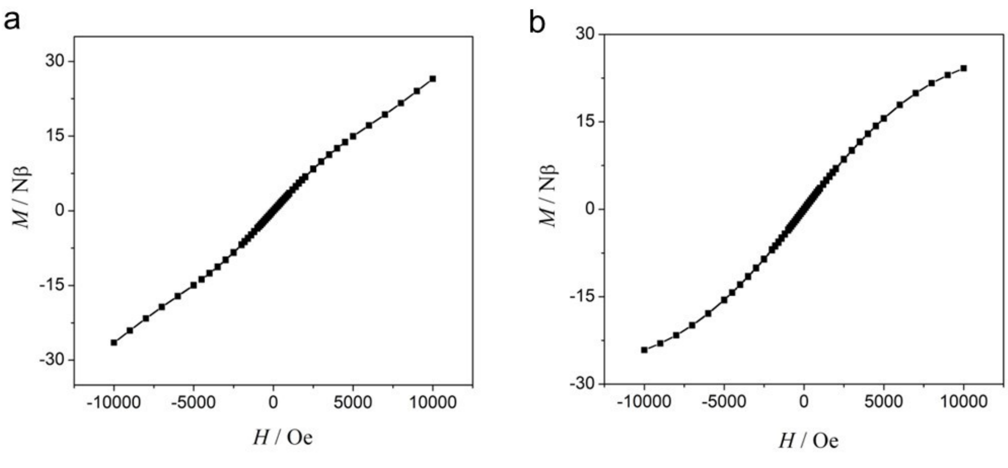

Figure S17. Loop curve graph of clusters ***S*-1** and ***S*-2** (a, b) at 2 K.

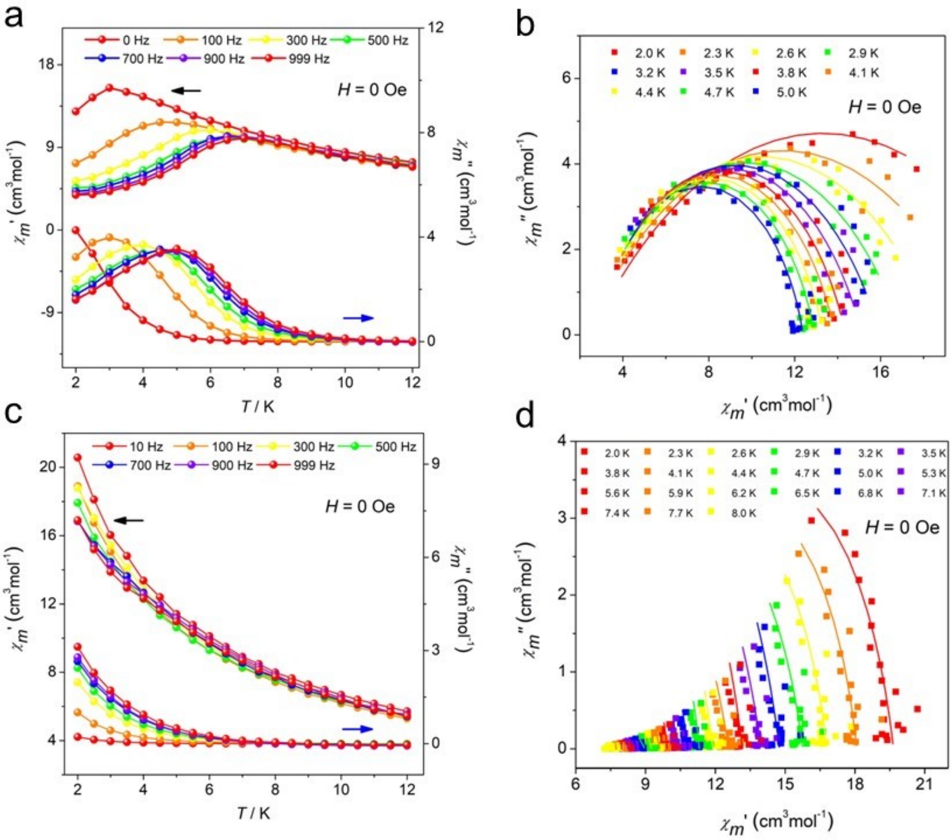

Figure S18. Temperature-dependent χ' and χ'' AC susceptibilities under 0 Oe DC fields for ***S*-1** and ***S*-2** (a, c); Cole−Cole plots for ***S*-1** and ***S*-2** (b, d).

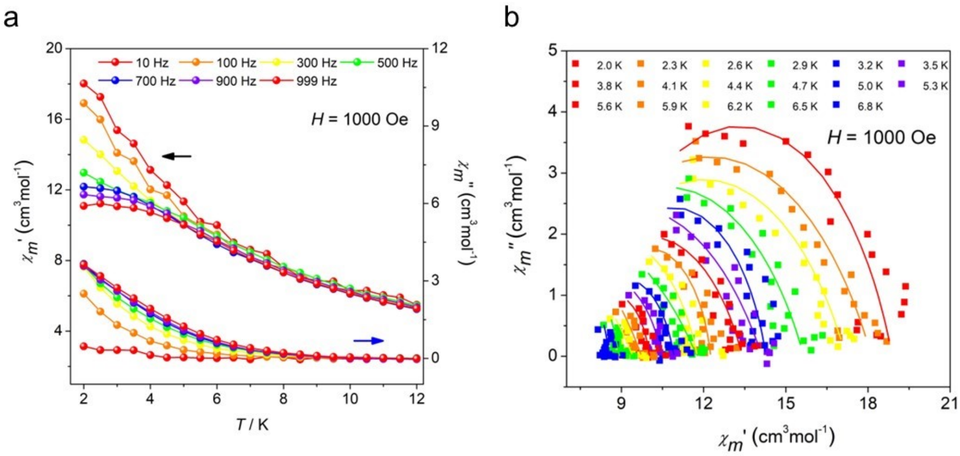

Figure S19. Temperature-dependent χ' and χ'' AC susceptibilities under 1000 Oe DC fields for ***S*-2** (a); Cole−Cole plots for ***S*-2** (b).

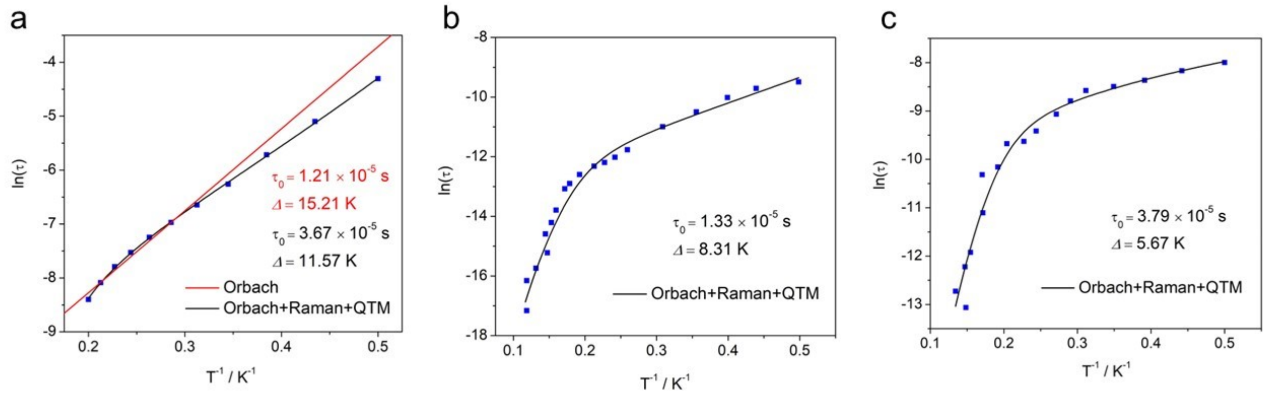

Figure S20. Arrhenius plots generated from the temperature-dependent relaxation times extracted from the Cole-Cole fits of the AC susceptibilities for clusters ***S*-1** and ***S*-2** under 0 Oe (a, b) and ***S*-2** under 1000 Oe (c). Symbols show the extracted times, and the lines are least-squares fits.

Table S2. Selected bond lengths (Å) and angles (°) of cluster ***R*-1**.

Bond lengths (Å)					
Dy1-O10	2.416(11)	Dy2-O3	2.330(11)	Dy3-N4	2.536(13)
Dy1-O17	2.361(15)	Dy2-O9	2.412(10)	Dy3-O15	2.372(12)
Dy1-O3	2.289(10)	Dy2-O11	2.327(9)	Dy4-O12	2.323(11)
Dy1-O2	2.395(11)	Dy2-O23	2.321(18)	Dy4-O10^i	2.335(10)
Dy1-O9	2.459(10)	Dy2-O33	2.586(5)	Dy4-O9^i	2.381(10)
Dy1-O8^i	2.271(11)	Dy3-O14	2.367(12)	Dy4-O11	2.381(10)
Dy1-N2	2.543(14)	Dy3-O12	2.417(10)	Dy4-O16	2.371(11)
Dy1-O18	2.345(12)	Dy3-O4	2.255(11)	Dy4-O7	2.348(10)
Dy2-O12	2.351(10)	Dy3-O6	2.359(12)	Dy4-O8	2.334(11)
Dy2-O10	2.317(10)	Dy3-O11	2.425(10)	Dy4-O33	2.632(5)
Dy2-O4	2.357(11)	Dy3-O7	2.245(10)		
Bond angles (°)					
O10-Dy1-O9	60.6(3)	O3-Dy2-O9	73.7(4)	O14-Dy3-O12	132.7(4)
O10-Dy1-N2	129.3(4)	O3-Dy2-O33	146.5(3)	O14-Dy3-O11	73.0(4)
O17-Dy1-O10	136.9(4)	O9-Dy2-O33	77.9(4)	O14-Dy3-N4	79.2(4)
O17-Dy1-O2	72.3(5)	O11-Dy2-O12	62.2(3)	O14-Dy3-O15	149.3(4)

O17-Dy1-O9	76.6(4)	O11-Dy2-O4	77.5(4)	O15-Dy3-O12	77.8(4)
O17-Dy1-N2	78.5(5)	O11-Dy2-O3	116.6(4)	O15-Dy3-O11	137.7(4)
O3-Dy1-O10	73.4(4)	O11-Dy2-O9	83.2(3)	O15-Dy3-N4	75.5(4)
O3-Dy1-O17	90.5(5)	O11-Dy2-O33	76.6(4)	O7-Dy3-N4	71.2(4)
O3-Dy1-O2	135.7(4)	O23-Dy2-O12	77.4(5)	O12-Dy4-O10^{i}	133.0(4)
O3-Dy1-O9	73.5(3)	O23-Dy2-O4	79.8(5)	O12-Dy4-O9^{i}	141.7(3)
O3-Dy1-N2	71.4(4)	O23-Dy2-O3	85.2(5)	O12-Dy4-O11	61.8(3)
O3-Dy1-O18	97.6(5)	O23-Dy2-O9	138.7(5)	O12-Dy4-O16	75.1(4)
O2-Dy1-O10	144.6(4)	O23-Dy2-O11	138.0(5)	O12-Dy4-O7	75.0(4)
O2-Dy1-O9	136.1(4)	O23-Dy2-O33	105.4(7)	O12-Dy4-O8	138.0(4)
O2-Dy1-N2	65.4(4)	O10-Dy2-O33	76.8(3)	O12-Dy4-O33	75.4(3)
O9-Dy1-N2	136.3(4)	O4-Dy2-O9	121.1(4)	O10^{i}-Dy4-O9^{i}	62.9(4)
O8^{i}-Dy1-O10	72.6(4)	O4-Dy2-O33	145.4(3)	O10^{i}-Dy4-O11	140.3(3)
O8^{i}-Dy1-O17	102.9(5)	O3-Dy2-O12	137.6(4)	O10^{i}-Dy4-O16	77.4(4)
O8^{i}-Dy1-O3	142.0(4)	O12-Dy3-O11	59.9(3)	O10^{i}-Dy4-O7	140.4(3)
O8^{i}-Dy1-O2	82.3(4)	O12-Dy3-N4	133.1(4)	O10^{i}-Dy4-O33	75.6(3)
O8^{i}-Dy1-O9	75.3(4)	O4-Dy3-O14	101.6(4)	O9^{i}-Dy4-O33	77.5(4)
O8^{i}-Dy1-N2	145.8(4)	O4-Dy3-O12	72.4(4)	O11-Dy4-O9^{i}	85.2(3)
O8^{i}-Dy1-O18	92.0(4)	O4-Dy3-O6	79.7(4)	O11-Dy4-O33	74.8(4)
O18-Dy1-O10	78.7(4)	O4-Dy3-O11	77.4(4)	O16-Dy4-O9^{i}	138.6(4)
O18-Dy1-O17	144.0(5)	O4-Dy3-N4	143.6(4)	O16-Dy4-O11	135.8(4)
O18-Dy1-O2	77.7(5)	O4-Dy3-O15	89.0(4)	O16-Dy4-O33	104.7(6)
O18-Dy1-O9	139.2(4)	O6-Dy3-O14	74.2(4)	O7-Dy4-O9^{i}	115.8(4)
O18-Dy1-N2	71.2(5)	O6-Dy3-O12	144.2(4)	O7-Dy4-O11	73.3(3)
O12-Dy2-O4	71.9(4)	O6-Dy3-O11	134.8(4)	O7-Dy4-O16	87.1(4)
O12-Dy2-O9	140.4(4)	O6-Dy3-N4	65.4(4)	O7-Dy4-O33	143.9(3)
O12-Dy2-O33	75.9(3)	O6-Dy3-O15	79.7(5)	O8-Dy4-O10^{i}	73.0(4)
O10-Dy2-O12	136.3(4)	O11-Dy3-N4	135.0(4)	O8-Dy4-O9^{i}	75.6(4)

O10-Dy2-O4	136.7(4)	O7-Dy3-O14	90.3(4)	O8-Dy4-O11	123.6(4)
O10-Dy2-O3	74.5(4)	O7-Dy3-O12	75.0(4)	O8-Dy4-O16	82.3(5)
O10-Dy2-O9	62.7(4)	O7-Dy3-O4	144.5(4)	O8-Dy4-O7	68.9(4)
O10-Dy2-O11	140.3(4)	O7-Dy3-O6	135.8(4)	O8-Dy4-O33	145.5(3)
O10-Dy2-O23	77.8(5)	O7-Dy3-O11	74.3(3)		
O3-Dy2-O4	67.1(4)	O7-Dy3-O15	97.6(5)		

Table S3. Selected bond lengths (Å) and angles (°) of cluster ***S*-1**.

Bond lengths (Å)					
Dy1-O11	2.454(6)	Dy2-O9	2.318(6)	Dy3-O7	2.262(5)
Dy1-O12	2.440(7)	Dy2-O10	2.365(6)	Dy3-O15	2.393(7)
Dy1-O2^{i}	2.353(7)	Dy2-O8	2.328(6)	Dy4-O11^{i}	2.399(6)
Dy1-O18	2.322(9)	Dy2-O7	2.346(6)	Dy4-O12^{i}	2.322(6)
Dy1-O3^{i}	2.273(6)	Dy2-O13	2.632(3)	Dy4-O9	2.358(6)
Dy1-O8	2.277(6)	Dy3-O16	2.347(7)	Dy4-O4	2.355(6)
Dy1-N2^{i}	2.533(8)	Dy3-O9	2.440(6)	Dy4-O10	2.317(5)
Dy1-O19	2.352(8)	Dy3-O4	2.246(6)	Dy4-O3	2.342(6)
Dy2-O11	2.365(6)	Dy3-N4	2.489(7)	Dy4-O13	2.587(3)
Dy2-O17	2.381(8)	Dy3-O10	2.438(6)	Dy4-O14	2.388(9)
Dy2-O12	2.348(6)	Dy3-O6	2.351(6)		
Bond angles (°)					
O3^{i}-Dy1-O18	90.5(3)	O9-Dy2-O12	131.9(2)	O7-Dy3-O9	74.7(2)
O3^{i}-Dy1-O8	141.9(2)	O9-Dy2-O10	62.5(2)	O7-Dy3-N4	71.4(2)
O3^{i}-Dy1-N2^{i}	71.1(2)	O9-Dy2-O8	137.8(2)	O7-Dy3-O10	74.40(19)
O3^{i}-Dy1-O19	97.4(3)	O9-Dy2-O7	75.5(2)	O7-Dy3-O6	136.0(2)
O8-Dy1-O11	75.2(2)	O9-Dy2-O13	75.11(17)	O7-Dy3-O15	97.1(3)
O8-Dy1-O12	72.3(2)	O10-Dy2-O17	136.0(2)	O15-Dy3-O9	77.4(2)
O8-Dy1-O2^{i}	82.5(2)	O10-Dy2-O13	74.9(2)	O15-Dy3-N4	74.5(2)

O8-Dy1-O18	103.8(3)	O8-Dy2-O11	76.0(2)	O15-Dy3-O10	137.2(2)
O8-Dy1-N2^{i}	145.9(2)	O8-Dy2-O17	82.2(3)	O11^{i}-Dy4-O13	78.1(2)
O8-Dy1-O19	90.6(3)	O8-Dy2-O12	73.1(2)	O12^{i}-Dy4-O11^{i}	63.1(2)
O19-Dy1-O11	137.4(2)	O8-Dy2-O10	124.0(2)	O12^{i}-Dy4-O9	135.2(2)
O19-Dy1-O12	76.7(3)	O8-Dy2-O7	68.41(19)	O12^{i}-Dy4-O4	136.5(2)
O19-Dy1-O2^{i}	78.3(3)	O8-Dy2-O13	145.66(15)	O12^{i}-Dy4-O3	74.5(2)
O19-Dy1-N2^{i}	72.4(3)	O7-Dy2-O11	116.2(2)	O12^{i}-Dy4-O13	76.79(17)
O11-Dy1-N2^{i}	136.7(2)	O7-Dy2-O17	87.0(3)	O12^{i}-Dy4-O14	76.3(3)
O12-Dy1-O11	60.7(2)	O7-Dy2-O12	139.79(19)	O9-Dy4-O11^{i}	140.6(2)
O12-Dy1-N2^{i}	128.7(2)	O7-Dy2-O10	74.3(2)	O9-Dy4-O13	75.37(17)
O2^{i}-Dy1-O11	136.7(2)	O7-Dy2-O13	144.66(14)	O9-Dy4-O14	77.4(3)
O2^{i}-Dy1-O12	143.9(3)	O16-Dy3-O9	133.2(2)	O4-Dy4-O11^{i}	122.0(2)
O2^{i}-Dy1-N2^{i}	65.5(2)	O16-Dy3-N4	80.2(2)	O4-Dy4-O9	71.8(2)
O18-Dy1-O11	77.4(2)	O16-Dy3-O10	73.5(2)	O4-Dy4-O13	145.08(14)
O18-Dy1-O12	137.7(2)	O16-Dy3-O6	74.2(2)	O4-Dy4-O14	80.1(4)
O18-Dy1-O2^{i}	72.6(3)	O16-Dy3-O15	149.3(2)	O10-Dy4-O11^{i}	83.2(2)
O18-Dy1-N2^{i}	78.4(3)	O9-Dy3-N4	132.2(2)	O10-Dy4-O12^{i}	140.6(2)
O18-Dy1-O19	145.2(3)	O4-Dy3-O16	102.0(3)	O10-Dy4-O9	62.7(2)
O3^{i}-Dy1-O11	73.8(2)	O4-Dy3-O9	72.2(2)	O10-Dy4-O4	78.0(2)
O3^{i}-Dy1-O12	73.5(2)	O4-Dy3-N4	143.2(2)	O10-Dy4-O3	116.8(2)
O3^{i}-Dy1-O2^{i}	135.6(2)	O4-Dy3-O10	77.6(2)	O10-Dy4-O13	76.6(2)
O11-Dy2-O17	138.3(2)	O4-Dy3-O6	79.7(2)	O10-Dy4-O14	138.7(3)
O11-Dy2-O10	85.2(2)	O4-Dy3-O7	144.3(2)	O3-Dy4-O11^{i}	73.6(2)
O11-Dy2-O13	77.8(2)	O4-Dy3-O15	88.5(3)	O3-Dy4-O9	138.1(2)
O17-Dy2-O13	103.6(3)	O10-Dy3-O9	59.8(2)	O3-Dy4-O4	67.7(2)
O12-Dy2-O11	63.3(2)	O10-Dy3-N4	136.1(2)	O3-Dy4-O13	146.40(17)
O12-Dy2-O17	76.6(2)	O6-Dy3-O9	143.8(2)	O3-Dy4-O14	85.6(4)
O12-Dy2-O10	140.4(2)	O6-Dy3-N4	65.5(2)	O14-Dy4-O11^{i}	137.9(3)

O12-Dy2-O13	75.45(17)	O6-Dy3-O10	135.2(2)	O14-Dy4-O13	104.2(5)
O9-Dy2-O11	142.1(2)	O6-Dy3-O15	79.6(3)		
O9-Dy2-O17	74.5(2)	O7-Dy3-O16	90.9(3)		

Table S4. Selected bond lengths (Å) and angles (°) of cluster ***R*-2**.

Bond lengths (Å)					
Dy1-O5	2.446(7)	Dy2-O12	2.292(6)	Dy3-O9^{i}	2.377(6)
Dy1-O12	2.365(6)	Dy2-O3	2.435(6)	Dy3-O10	2.382(5)
Dy1-O3	2.246(6)	Dy2-O11	2.366(5)	Dy3-O10^{i}	2.543(6)
Dy1-O14	2.290(7)	Dy2-N4	2.431(7)	Dy3-O11	2.305(5)
Dy1-O6	2.391(6)	Dy2-O4	2.301(6)	Dy3-O16	2.480(7)
Dy1-N2	2.513(9)	Dy2-O15	2.438(7)	Dy3-N6	2.517(8)
Dy1-O2	2.358(7)	Dy2-O6	2.368(5)	Dy3-O17	2.428(7)
Dy1-O13	2.392(10)	Dy3-O7	2.423(5)		
Dy2-O7	2.277(5)	Dy3-O8	2.293(6)		
Bond angles (°)					
O5-Dy1-N2	78.1(2)	O7-Dy2-N4	76.2(2)	O8-Dy3-O10^{i}	70.06(19)
O12-Dy1-O5	134.9(2)	O7-Dy2-O4	77.4(2)	O8-Dy3-O10	76.34(18)
O12-Dy1-O6	70.1(2)	O7-Dy2-O15	81.4(2)	O8-Dy3-O11	134.9(2)
O12-Dy1-N2	130.9(2)	O7-Dy2-O6	133.6(2)	O8-Dy3-O16	74.8(2)
O12-Dy1-O13	74.7(3)	O12-Dy2-O3	69.3(2)	O8-Dy3-N6	128.9(2)
O3-Dy1-O5	94.2(2)	O12-Dy2-O11	70.7(2)	O8-Dy3-O17	141.6(2)
O3-Dy1-O12	71.3(2)	O12-Dy2-N4	137.8(2)	O9^{i}-Dy3-O7	71.9(2)
O3-Dy1-O14	143.8(2)	O12-Dy2-O4	114.0(2)	O9^{i}-Dy3-O10	124.0(2)
O3-Dy1-O6	68.2(2)	O12-Dy2-O15	84.3(2)	O9^{i}-Dy3-O10^{i}	61.66(17)
O3-Dy1-N2	71.0(2)	O12-Dy2-O6	71.8(2)	O9^{i}-Dy3-O16	147.8(2)
O3-Dy1-O2	135.9(3)	O3-Dy2-O15	133.4(2)	O9^{i}-Dy3-N6	140.7(3)
O3-Dy1-O13	95.5(4)	O11-Dy2-O3	124.4(2)	O9^{i}-Dy3-O17	70.2(3)

O14-Dy1-O5	87.4(2)	O11-Dy2-N4	145.5(2)	O10-Dy3-O7	139.4(2)
O14-Dy1-O12	82.1(2)	O11-Dy2-O15	77.4(2)	O10-Dy3-O10[i]	62.4(2)
O14-Dy1-O6	80.1(2)	O11-Dy2-O6	131.9(2)	O10-Dy3-O16	78.8(2)
O14-Dy1-N2	143.8(2)	N4-Dy2-O3	88.9(2)	O10-Dy3-N6	64.3(2)
O14-Dy1-O2	79.0(2)	N4-Dy2-O15	85.8(2)	O10-Dy3-O17	89.8(2)
O14-Dy1-O13	100.8(4)	O4-Dy2-O3	66.41(19)	O11-Dy3-O7	70.2(2)
O6-Dy1-O5	64.95(19)	O4-Dy2-O11	97.8(2)	O11-Dy3-O9[i]	90.2(2)
O6-Dy1-N2	121.2(3)	O4-Dy2-N4	87.0(2)	O11-Dy3-O10	137.5(2)
O6-Dy1-O13	144.4(3)	O4-Dy2-O15	158.7(2)	O11-Dy3-O10[i]	144.1(2)
O2-Dy1-O5	72.9(3)	O4-Dy2-O6	124.61(19)	O11-Dy3-O16	83.5(2)
O2-Dy1-O12	145.3(3)	O6-Dy2-O3	65.6(2)	O11-Dy3-N6	73.2(2)
O2-Dy1-O6	133.4(2)	O6-Dy2-N4	66.3(2)	O11-Dy3-O17	78.2(2)
O2-Dy1-N2	65.1(3)	O6-Dy2-O15	70.0(2)	O16-Dy3-O10[i]	132.3(2)
O2-Dy1-O13	80.6(3)	O7-Dy3-O10[i]	115.8(2)	O16-Dy3-N6	66.9(3)
O13-Dy1-O5	150.3(3)	O7-Dy3-O16	76.3(2)	N6-Dy3-O10[i]	113.8(2)
O13-Dy1-N2	78.6(4)	O7-Dy3-N6	130.2(2)	O17-Dy3-O10[i]	71.8(2)
O7-Dy2-O12	141.8(2)	O7-Dy3-O17	129.8(2)	O17-Dy3-O16	137.9(3)
O7-Dy2-O3	141.5(2)	O8-Dy3-O7	66.47(17)	O17-Dy3-N6	71.6(3)
O7-Dy2-O11	71.69(19)	O8-Dy3-O9[i]	88.1(2)		

Table S5. Selected bond lengths (Å) and angles (°) of cluster ***S*-2**.

Bond lengths (Å)					
Dy1-O12	2.370(5)	Dy2-O12	2.294(5)	Dy3-O9[i]	2.378(6)
Dy1-O5	2.438(6)	Dy2-O15	2.428(6)	Dy3-O10	2.373(4)
Dy1-O3	2.248(6)	Dy2-O11	2.358(5)	Dy3-O10[i]	2.554(5)
Dy1-O14	2.282(6)	Dy2-O3	2.434(5)	Dy3-O11	2.314(4)
Dy1-O6	2.405(5)	Dy2-O4	2.299(5)	Dy3-O16	2.456(7)
Dy1-O2	2.352(6)	Dy2-O6	2.379(5)	Dy3-N6	2.517(7)

Dy1-N2	2.552(8)	Dy2-N4	2.421(7)	Dy3-O17	2.414(7)
Dy1-O13	2.391(9)	Dy3-O7	2.427(5)		
Dy2-O7	2.289(4)	Dy3-O8	2.300(5)		
Bond angles (°)					
O12-Dy1-O5	135.23(18)	O7-Dy2-O3	141.6(2)	O8-Dy3-O10	76.46(17)
O12-Dy1-O6	70.45(18)	O7-Dy2-O4	77.68(19)	O8-Dy3-O11	134.50(18)
O12-Dy1-N2	131.0(2)	O7-Dy2-O6	133.08(19)	O8-Dy3-O16	75.0(2)
O12-Dy1-O13	74.6(2)	O7-Dy2-N4	76.17(18)	O8-Dy3-N6	128.6(2)
O5-Dy1-N2	77.5(2)	O12-Dy2-O15	84.4(2)	O8-Dy3-O17	142.3(2)
O3-Dy1-O12	71.5(2)	O12-Dy2-O11	70.51(17)	$O9^{i}$-Dy3-O7	71.71(19)
O3-Dy1-O5	93.8(2)	O12-Dy2-O3	69.6(2)	$O9^{i}$-Dy3-$O10^{i}$	61.91(16)
O3-Dy1-O14	143.30(19)	O12-Dy2-O4	113.9(2)	$O9^{i}$-Dy3-O16	147.6(2)
O3-Dy1-O6	68.0(2)	O12-Dy2-O6	72.20(19)	$O9^{i}$-Dy3-N6	141.2(2)
O3-Dy1-O2	136.3(2)	O12-Dy2-N4	137.80(19)	$O9^{i}$-Dy3-O17	70.9(2)
O3-Dy1-N2	71.0(2)	O15-Dy2-O3	133.32(18)	O10-Dy3-O7	139.19(18)
O3-Dy1-O13	95.3(4)	O11-Dy2-O15	77.2(2)	O10-Dy3-$O9^{i}$	124.37(18)
O14-Dy1-O12	82.1(2)	O11-Dy2-O3	124.8(2)	O10-Dy3-$O10^{i}$	62.5(2)
O14-Dy1-O5	87.2(2)	O11-Dy2-O6	131.89(19)	O10-Dy3-O16	78.8(2)
O14-Dy1-O6	79.5(2)	O11-Dy2-N4	145.56(19)	O10-Dy3-N6	64.27(18)
O14-Dy1-O2	79.0(2)	O4-Dy2-O15	158.67(19)	O10-Dy3-O17	89.7(2)
O14-Dy1-N2	144.01(18)	O4-Dy2-O11	98.08(19)	O11-Dy3-O7	70.13(19)
O14-Dy1-O13	101.8(4)	O4-Dy2-O3	66.42(17)	O11-Dy3-$O9^{i}$	90.20(19)
O6-Dy1-O5	64.88(16)	O4-Dy2-O6	124.55(17)	O11-Dy3-O10	137.36(19)
O6-Dy1-N2	120.8(2)	O4-Dy2-N4	87.0(2)	O11-Dy3-$O10^{i}$	144.37(19)
O2-Dy1-O12	145.0(3)	O6-Dy2-O15	69.94(18)	O11-Dy3-O16	82.9(2)
O2-Dy1-O5	73.0(3)	O6-Dy2-O3	65.53(18)	O11-Dy3-N6	73.13(18)
O2-Dy1-O6	133.2(2)	O6-Dy2-N4	65.9(2)	O11-Dy3-O17	78.2(2)
O2-Dy1-N2	65.5(2)	N4-Dy2-O15	85.8(2)	O16-Dy3-$O10^{i}$	132.58(18)

O2-Dy1-O13	80.8(3)	N4-Dy2-O3	88.5(2)	O16-Dy3-N6	66.3(2)
O13-Dy1-O5	150.1(2)	O7-Dy3-O10^{i}	115.86(19)	N6-Dy3-O10^{i}	114.0(2)
O13-Dy1-O6	144.5(2)	O7-Dy3-O16	76.21(19)	O17-Dy3-O7	130.1(2)
O13-Dy1-N2	78.7(3)	O7-Dy3-N6	129.8(2)	O17-Dy3-O10^{i}	72.2(2)
O7-Dy2-O12	141.73(19)	O8-Dy3-O7	66.23(16)	O17-Dy3-O16	137.1(3)
O7-Dy2-O15	81.1(2)	O8-Dy3-O9^{i}	88.1(2)	O17-Dy3-N6	71.4(3)
O7-Dy2-O11	71.80(18)	O8-Dy3-O10^{i}	70.30(18)		

Table S6. *SHAPE* analysis of the Dy(III) in cluster ***R*-1**.

Label	**Shape**	**Symmetry**	**Distortion** (°)			
			Dy1	**Dy2**	**Dy3**	**Dy4**
OP-8	D_{8h}	Octagon	29.039	26.380	28.903	25.933
HPY-8	C_{7v}	Heptagonal pyramid	23.562	20.673	24.159	21.238
HBPY-8	D_{6h}	Hexagonal bipyramid	15.482	16.685	15.109	16.540
CU-8	O_h	Cube	12.733	11.994	12.535	12.412
SAPR-8	D_{4d}	Square antiprism	2.343	1.381	2.549	1.405
TDD-8	D_{2d}	Triangular dodecahedron	0.988	2.007	1.144	2.157
JGBF-8	D_{2d}	Johnson-Gyrobifastigium (J26)	11.566	15.608	11.001	14.908
JETBPY-8	D_{3h}	Johnson-Elongated triangular bipyramid (J14)	26.905	25.956	27.183	26.131
JBTP-8	C_{2v}	Johnson-Biaugmented trigonal prism (J50)	2.272	2.874	2.349	2.707
BTPR-8	C_{2v}	Biaugmented trigonal prism	2.007	1.780	2.101	1.679
JSD-8	D_{2d}	Snub disphenoid (J84)	2.074	4.669	2.142	4.537
TT-8	T_d	Triakis tetrahedron	13.451	12.327	13.230	12.891
ETBPY-8	D_{3h}	Elongated trigonal bipyramid	23.431	21.220	23.916	21.790

Table S7. *SHAPE* analysis of the Dy(III) in cluster ***S*-1**.

Label	Shape	Symmetry	Distortion (°)			
			Dy1	**Dy2**	**Dy3**	**Dy4**
OP-8	D_{8h}	Octagon	28.913	26.853	28.939	26.120
HPY-8	C_{7v}	Heptagonal pyramid	23.556	20.752	23.962	21.381
HBPY-8	D_{6h}	Hexagonal bipyramid	15.551	16.618	14.923	16.306
CU-8	O_h	Cube	12.685	11.874	12.407	12.373
SAPR-8	D_{4d}	Square antiprism	2.2853	1.434	2.516	1.387
TDD-8	D_{2d}	Triangular dodecahedron	0.997	1.894	1.179	2.046
JGBF-8	D_{2d}	Johnson-Gyrobifastigium (J26)	11.671	15.434	10.862	14.732
JETBPY-8	D_{3h}	Johnson-Elongated triangular bipyramid (J14)	26.883	26.364	27.075	26.640
JBTP-8	C_{2v}	Johnson-Biaugmented trigonal prism (J50)	2.198	2.805	2.409	2.698
BTPR-8	C_{2v}	Biaugmented trigonal prism	1.937	1.679	2.157	1.619
JSD-8	D_{2d}	Snub disphenoid (J84)	2.095	4.595	2.104	4.471
TT-8	T_d	Triakis tetrahedron	13.408	12.213	13.174	12.825
ETBPY-8	D_{3h}	Elongated trigonal bipyramid(see8)	23.374	21.678	23.815	22.345

Table S8. *SHAPE* analysis of the Dy(III) in cluster ***R*-2**.

Label	Shape	Symmetry	Distortion (°)	
			Dy1	**Dy2**
OP-8	D_{8h}	Octagon	30.797	31.379
HPY-8	C_{7v}	Heptagonal pyramid	23.531	23.404
HBPY-8	D_{6h}	Hexagonal bipyramid	16.395	13.466
CU-8	O_h	Cube	11.640	12.415
SAPR-8	D_{4d}	Square antiprism	3.024	3.501
TDD-8	D_{2d}	Triangular dodecahedron	0.898	2.599

JGBF-8	D_{2d}	Johnson-Gyrobifastigium (J26)	12.666	10.371
JETBPY-8	D_{3h}	Johnson-Elongated triangular bipyramid (J14)	29.434	27.263
JBTP-8	C_{2v}	Johnson-Biaugmented trigonal prism (J50)	3.148	2.912
BTPR-8	C_{2v}	Biaugmen tedtrigonal prism	2.696	1.767
JSD-8	D_{2d}	Snub disphenoid (J84)	2.747	4.335
TT-8	T_d	Triakis tetrahedron	12.372	13.149
ETBPY-8	D_{3h}	Elongated trigonal bipyramid	24.815	22.827

Label	**Shape**	**Symmetry**	**Distortion** (°)
			Dy3
EP-9	D_{9h}	Enneagon	34.168
OPY-9	C_{8v}	Octagonal pyramid	22.796
HBPY-9	D_{7h}	Heptagonal bipyramid	17.267
JTC-9	C_{3v}	Triangular cupola J3	15.016
JCCU-9	C_{4v}	Capped cube (J8)	8.664
CCU-9	C_4	Capped cube	7.378
JCSAPR-9	C_{4v}	Capped sq. antiprism	2.254
CSAPR-9	C_{4v}	Capped square antiprism	1.229
JTCTPR-9	D_{3h}	Tricapped trigonal prism J51	2.012
TCTPR-9	D_{3h}	Tricapped trigonal prism	1.251
JTDIC-9	C_{3v}	Tridiminished icosahedron J63	12.771
HH-9	C_{2v}	Hula-hoop	10.110
MFF-9	C_s	Muffin	1.335

Table S9. *SHAPE* analysis of the Dy(III) in cluster ***S*-2**.

Label	**Shape**	**Symmetry**	**Distortion** (°)	
			Dy1	**Dy2**
OP-8	D_{8h}	Octagon	30.940	31.285

HPY-8	C_{7v}	Heptagonal pyramid	23.682	23.506
HBPY-8	D_{6h}	Hexagonal bipyramid	16.282	13.509
CU-8	O_h	Cube	11.733	12.523
SAPR-8	D_{4d}	Square antiprism	3.081	3.505
TDD-8	D_{2d}	Triangular dodecahedron	0.887	2.627
JGBF-8	D_{2d}	Johnson-Gyrobifastigium (J26)	12.734	10.331
JETBPY-8	D_{3h}	Johnson-Elongated triangular bipyramid (J14)	29.067	27.142
JBTP-8	C_{2v}	Johnson-Biaugmented trigonal prism (J50)	3.178	2.954
BTPR-8	C_{2v}	Biaugmen tedtrigonal prism	2.549	1.832
JSD-8	D_{2d}	Snub disphenoid (J84)	2.561	4.313
TT-8	T_d	Triakis tetrahedron	12.410	13.212
ETBPY-8	D_{3h}	Elongated trigonal bipyramid	25.398	22.628

Label	**Shape**	**Symmetry**	**Distortion** (°) **Dy3**
EP-9	D_{9h}	Enneagon	34.183
OPY-9	C_{8v}	Octagonal pyramid	22.825
HBPY-9	D_{7h}	Heptagonal bipyramid	17.247
JTC-9	C_{3v}	Triangular cupola J3	15.035
JCCU-9	C_{4v}	Capped cube (J8)	8.579
CCU-9	C_4	Capped cube	7.350
JCSAPR-9	C_{4v}	Capped sq. antiprism	2.255
CSAPR-9	C_{4v}	Capped square antiprism	1.227
JTCTPR-9	D_{3h}	Tricapped trigonal prism J51	1.961
TCTPR-9	D_{3h}	Tricapped trigonal prism	1.257
JTDIC-9	C_{3v}	Tridiminished icosahedron J63	12.762

HH-9	C_{2v}	Hula-hoop	10.137
MFF-9	C_s	Muffin	1.314

Table S10. Parameters from the fitting result of the Cole-Cole plots for the ***R*-1** under 0 Oe field.

	***R*-1**		
*T*emp.(K)	*τ*	*α*	residual
5.0	0.296032E-03	0.244656E+00	0.143606E+00
4.7	0.396460E-03	0.264993E+00	0.191508E+00
4.4	0.531762E-03	0.285873E+00	0.243871E+00
4.1	0.715844E-03	0.303777E+00	0.318819E+00
3.8	0.966411E-03	0.323445E+00	0.380225E+00
3.5	0.131679E-02	0.344271E+00	0.453641E+00
3.2	0.187588E-02	0.364864E+00	0.525670E+00
2.9	0.285038E-02	0.388242E+00	0.584445E+00
2.6	0.466894E-02	0.413761E+00	0.887917E+00
2.3	0.851159E-02	0.446712E+00	0.550999E+00
2.0	0.169600E-01	0.490874E+00	0.394759E+00

Table S11. Parameters from the fitting result of the Cole-Cole plots for the ***R*-2** under 0 Oe field.

	***R*-2**		
*T*emp.(K)	*τ*	*α*	residual
2.0	0.185721E-03	0.305145E+00	0.702823E-01
2.5	0.174744E-03	0.273494E+00	0.682148E-01
3.0	0.165713E-03	0.256340E+00	0.588019E-01
3.5	0.158271E-03	0.244586E+00	0.545725E-01
4.0	0.150792E-03	0.236670E+00	0.456045E-01
4.5	0.141043E-03	0.234421E+00	0.352555E-01
5.0	0.132836E-03	0.227043E+00	0.328097E-01
5.5	0.123869E-03	0.222413E+00	0.263064E-01
6.0	0.113927E-03	0.215366E+00	0.218576E-01
6.5	0.102865E-03	0.211176E+00	0.156278E-01
7.0	0.924204E-04	0.204779E+00	0.118463E-01
7.5	0.632913E-06	0.691005E+00	0.365156E+01
8.0	0.516291E-05	0.337087E+00	0.127491E-01
8.5	0.396282E-05	0.313579E+00	0.767048E-02
9.0	0.303176E-05	0.287576E+00	0.500746E-02
9.5	0.233652E-05	0.254981E+00	0.396000E-02
10.0	0.124680E-05	0.280504E+00	0.839930E-01

Table S12. Parameters from the fitting result of the Cole-Cole plots for the ***R*-2** under 1000 Oe field.

	***R*-2**		
*T*emp.(K)	τ	α	residual
2.0	0.541202E-03	0.309313E+00	0.331614E+00
2.5	0.431551E-03	0.298966E+00	0.191431E+00
3.0	0.355077E-03	0.307415E+00	0.923385E+00
3.5	0.317890E-03	0.281377E+00	0.101769E+00
4.0	0.293437E-03	0.249301E+00	0.590389E+00
4.5	0.233407E-03	0.275505E+00	0.937777E+00
5.0	0.218947E-03	0.240321E+00	0.811918E-01
5.5	0.116915E-03	0.376318E+00	0.500788E+01
6.0	0.155960E-03	0.237343E+00	0.364479E-01
6.5	0.136306E-03	0.218145E+00	0.321418E-01
7.0	0.112108E-03	0.216957E+00	0.229871E-01
7.5	0.131769E-03	0.437632E+00	0.468881E+01
8.0	0.182822E-03	0.505731E+00	0.488010E-01
8.5	0.155999E-03	0.102493E+00	0.406885E-01
9.0	0.204887E-03	0.129780E+00	0.440238E+00
9.5	0.127147E-03	0.510891E+00	0.448092E-01
10.0	0.928791E-04	0.130480E+00	0.105949E-01

Table S13. Parameters from the fitting result of the Cole-Cole plots for the ***S*-1** under 0 Oe field.

	***S*-1**		
*T*emp.(K)	τ	α	residual
2.0	0.135298E-01	0.476624E+00	0.271138E+01
2.3	0.610367E-02	0.440763E+00	0.413320E+01
2.6	0.328692E-02	0.400390E+00	0.187731E+01
2.9	0.191202E-02	0.359570E+00	0.303056E+01
3.2	0.129758E-02	0.322138E+00	0.338158E+01
3.5	0.938169E-03	0.291340E+00	0.307369E+01
3.8	0.712833E-03	0.256317E+00	0.311767E+01
4.1	0.538181E-03	0.246634E+00	0.243062E+01
4.4	0.413947E-03	0.218830E+00	0.294600E+01
4.7	0.307372E-03	0.211419E+00	0.232269E+01
5.0	0.224999E-03	0.188957E+00	0.214014E+01

Table S14. Parameters from the fitting result of the Cole-Cole plots for the ***S*-2** under 0 Oe field.

	***S*-2**

*T*emp.(K)	τ	α	residual
2.0	0.880020E-04	0.225023E+00	0.361788E+01
2.3	0.706370E-04	0.206747E+00	0.267288E+01
2.6	0.523292E-04	0.214592E+00	0.278556E+01
2.9	0.345059E-04	0.246159E+00	0.210347E+01
3.2	0.132563E-04	0.250346E+00	0.236751E+01
3.5	0.802929E-05	0.282038E+00	0.170793E+01
3.8	0.770223E-05	0.234678E+00	0.185850E+01
4.1	0.476622E-05	0.299269E+00	0.136504E+01
4.4	0.506427E-05	0.235104E+00	0.123434E+01
4.7	0.446807E-05	0.215544E+00	0.130343E+01
5.0	0.337152E-05	0.235373E+00	0.153139E+01
5.3	0.230348E-05	0.271925E+00	0.135585E+01
5.6	0.249579E-05	0.208922E+00	0.992459E+00
5.9	0.609087E-06	0.393802E+00	0.738501E+00
6.2	0.248039E-06	0.468510E+00	0.109518E+01
6.5	0.445975E-08	0.672717E+00	0.110266E+01
6.8	0.101401E-06	0.487992E+00	0.865128E+00
7.1	0.710081E-06	0.239767E+00	0.628120E+00
7.4	0.115485E-05	0.111022E+00	0.710321E+00
7.7	0.429028E-06	0.229864E+00	0.749382E+00
8.0	0.628262E-07	0.392412E+00	0.513175E+00

Table S15. Parameters from the fitting result of the Cole-Cole plots for the ***S*-2** under 1000 Oe field.

	***S*-2**		
*T*emp.(K)	τ	α	residual
2.0	0.336352E-03	0.245833E+00	0.632162E+01
2.3	0.242788E-03	0.353511E+00	0.439253E+01
2.6	0.238893E-03	0.350188E+00	0.252197E+01
2.9	0.140517E-03	0.347542E+00	0.459260E+01
3.2	0.180169E-03	0.199521E+00	0.280702E+01
3.5	0.719531E-04	0.398869E+00	0.296640E+01
3.8	0.121984E-03	0.325708E+00	0.200484E+01
4.1	0.146031E-03	0.145569E+00	0.242994E+01
4.4	0.658355E-04	0.266245E+00	0.348647E+01
4.7	0.123830E-04	0.480555E+00	0.215046E+01
5.0	0.949058E-04	0.214635E+00	0.163073E+01
5.3	0.591531E-04	0.260118E+00	0.226805E+01
5.6	0.832576E-04	0.169373E+00	0.125811E+01
5.9	0.344110E-05	0.430653E+00	0.169145E+01
6.2	0.212198E-05	0.461314E+00	0.133442E+01

6.5	0.496981E-05	0.259048E+00	0.169675E+01
6.8	0.492712E-05	0.210584E+00	0.845698E+00